

The concept of selectivity control by simultaneous distribution of the oxygen feed and wall temperature in a microstructured reactor

Samson M. Aworinde,^a Artur M. Schweidtmann,^{a,b} Alexei A. Lapkin^{a,c,*}

^a *Department of Chemical Engineering and Biotechnology, University of Cambridge,
Philippa Fawcett Drive, Cambridge CB3 0AS, United Kingdom*

^b *Aachener Verfahrenstechnik – Process Systems Engineering, RWTH Aachen University,
Aachen, Germany*

^c *Cambridge Centre for Advanced Research and Education in Singapore Ltd. 1 Create Way,
CREATE Tower #05-05, 138602 Singapore*

Abstract

This paper explores the feasibility of controlling the selectivity of a partial oxidation reaction by simultaneous modulation of local oxygen concentration and coolant temperature along the length of a reactor. The microstructured membrane reactor (MMR) concept consists of an oxygen-permeable membrane for distributing the oxygen feed with the coolant channel divided into zones of different temperatures. The reactor concept was explored in simulation of the selective oxidation of *o*-xylene to phthalic anhydride (PA). A mathematical model of the reactor was developed and optimization performed with the objective of maximising PA selectivity at the reactor outlet. Dosing of oxygen at uniform wall temperature results in PA selectivity increase by 6.3%, albeit with a reduction in *o*-xylene conversion of about 8% compared to a conventional fixed bed reactor. However, simultaneous modulation of both reactor wall temperatures and local oxygen

* Corresponding author. E-mail address: aal35@cam.ac.uk (A.A. Lapkin)

concentration results in an improved conversion of *o*-xylene without a detrimental effect on selectivity, thus giving maximum yield of PA.

Keywords: Selective oxidation; Selectivity; Microreactor; Membrane; *o*-Xylene; Optimization

1. Introduction

One of the key challenges in many catalytic selective oxidations is poor selectivity of the desired product [1]. Over-oxidation of the desired product as well as total oxidation of the hydrocarbon substrate account for the loss in selectivity, and in most oxidation processes about 10-30% of feed is lost as carbon oxides. For large scale oxidation processes, there is a significant incentive to optimise selectivity, since even a small increase in selectivity can bring significant economic benefits through annual savings in raw material cost as well as the cost of downstream separation and purification of products [2]. Cost savings are hugely important to a petrochemical plant, considering that around 75% of the total production costs are typically allocated to feedstock [3]. The attendant reduction in CO_x formation and carbon emissions due to improved selectivity can also make many large-scale commercial oxidation processes more environmentally friendly [4]. In selective oxidations, there is usually a trade-off between product selectivity and conversion of the hydrocarbon; the conditions under which high selectivity can be attained typically correspond to regions of low conversion [5]. Thus, in attempting to improve process selectivity, there is the risk of unavoidable loss of conversion and, consequently, of product yield.

A number of strategies can lead to enhanced selectivity of catalytic oxidation reactions. The most significant is the development of new catalysts that are more selective for the desired product. However, catalysts on their own rarely determine the overall efficiency of a process, and there are

many oxidation reactions for which the desirable catalysts that are highly selective for the target product are still elusive [6]. Furthermore, the selectivity of a catalyst is intimately linked to its activity, productivity and stability, and often a new catalyst which gives a boost in selectivity may suffer from loss of activity and lower lifetime compared to conventional catalysts, thus requiring more frequent regeneration [7]. Thus, further strategies to improve selectivity are developed around engineering of the reaction environment, directed by detailed mechanistic understanding of the reaction pathways.

There is a potential to improve selectivity of oxidation reactions substituting molecular oxygen with lattice oxygen, in the process known as redox decoupling or “chemical looping” [8]. In this case the selective oxidation of a hydrocarbon substrate is done by lattice oxygen of a metal oxide catalyst, an oxygen carrier, in one reactor while the reduced solid is re-oxidised by contact with air in a separate reactor. The re-oxidised solid is subsequently cycled back to the oxidation reactor, thus the substrate and air are never in direct contact, minimising non-selective homogenous combustion reactions. This strategy has been implemented for example to improve propene selectivity in the oxidative dehydrogenation of propane over V_2O_5 - SiO_2 catalyst [9]. The cyclic approach requires development of a new type of a solid catalyst which has a high oxygen-carrying capacity per unit weight. In addition, the solid must have excellent stability and high resistant to attrition in multi-cycle operations.

The use of alternative oxidants such as H_2O_2 , N_2O and alkylhydroperoxides as substitutes for molecular oxygen have also been investigated for enhancing selectivity in certain reactions, such as the epoxidation of olefins [10] and oxidative dehydrogenation of alkanes to olefins [11]. However, the use of these alternative oxygen sources may be economically unfavourable due to

their high cost of production as well as storage and handling issues. Hence, in most commodity chemical processes, oxygen or air is still the preferred oxidant.

Another strategy may involve the use of protective groups that effectively remove the desired products from the reaction medium, thus preventing its over-oxidation. The concept of a protective agent has, for example, been applied in the boron-modified liquid-phase oxidation of alkanes and cycloalkanes into alcohols. In this case a boron compound is used as an esterifying agent to trap the alcohol by forming a borate ester, which is more stable to further oxidation, thus resulting in an improved alcohol selectivity [12,13]. Another example is the direct oxidation of methane to methanol in concentrated sulphuric acid using SO_3 as the oxidant and a Pt(II) complex as catalyst [14,15]. Methane is converted to methyl bisulphate ester from which methanol is obtained as the final product. In both cases, the desired alcohols are recovered by hydrolyzing the esters with water, with up to 80% final product selectivity.

The development of alternative process chemistry and innovative synthesis routes may also be a successful approach to improve selectivity of certain oxidation reactions. This may involve the use of alternative feedstock that requires fewer number of mechanistic steps and allows oxidation under mild conditions, thus producing less by-products than classical routes [16]. A good example where a change of synthesis route has turned out to be more selective is the production of methyl methacrylate (MMA). Conventional process uses C_4 feedstocks such as isobutylene or *t*-butanol and involves three steps: two high temperature gas-phase catalytic oxidations to methacrolein and methacrylic acid, respectively, followed by esterification of the acid with methanol into MMA [17]. In contrast, a new process developed by Asahi Chemical involves only two steps: isobutylene is first oxidised into methacrolein, followed by direct liquid-phase oxidative esterification into

MMA at low temperature with no intermediate formation of methacrylic acid. The new process has better selectivity to MMA, however, it also required the development of new catalysts [18]. Complementary to developing more selective catalysts and process chemistry is the reactor engineering approach, using the already available reaction routes and catalysts [19,20]. Many gas-phase selective oxidations are strongly exothermic and are, typically, carried out in multi-tubular packed bed reactors with external cooling. The efficiency of heat removal is the main challenge for these reactors. Limitations in radial heat transfer frequently leads to the development of hot spots in the catalyst bed, resulting in a decrease in selectivity. There has been a considerable effort in development of innovative reactor concepts that allow a more efficient heat transfer in fast exothermic reactions, typically following the idea of a reduction in thermal resistance by minimising the length-scale for heat transfer [21]. The small channel dimensions (typically 1–4 mm) result in a high surface-to-volume ratio and minimise transport limitations, leading to much improved heat and mass transfer compared to conventional macro scale reactors [22]. This makes meso-scale, or compact, reactors particularly suitable for fast exothermic chemical reactions that require efficient thermal management. Micro- and meso-scale reactors with efficient heat transfer were studied extensively in exothermic oxidation reactions, for example in epoxidation of propene [23], *n*-butane oxidation to maleic anhydride [24], oxidation of alcohols [25], and many others. Apart from temperature management, the control of oxygen concentration in an oxidation reactor can also be crucial for controlling the selectivity. In this respect, membrane reactors have been investigated for providing a means of achieving controlled oxygen dosing, for example in selective oxidations and oxidative dehydrogenation of alkanes [26]. The distributed feeding of oxygen along the reactor length ensures that the local concentration in contact with the hydrocarbon at any point in the reactor is lower than in the co-feed mode, thus minimising by-product formation [27,28].

Integrating the benefits of a compact reactor with membrane dosing presents a new opportunity for intensification of oxidation reactions as was investigated by Bortolotto and Dittmeyer [29] for the hydroxylation of benzene to phenol. As manufacturing technology develops and opens new possibilities to develop complex multi-dimensional non-uniform device architectures, it is worth re-visiting the approaches to reactor design and to explore new design freedoms for the purpose of attaining better reaction performance, compared to what had been feasible using conventional reactor technologies.

In the present paper, a concept microstructured reactor with spatial distribution of the oxygen feed and coolant temperature is investigated by means of process modelling and optimization. The objective is to maximise selectivity without detrimental effect on the product yield. The reactor concept is optimized to determine the configuration and operating conditions leading to best performance in terms of selectivity and yield. As a case study the highly exothermic selective oxidation of *o*-xylene to phthalic anhydride on vanadium-titanium catalyst, one of the most important synthesis reactions in the petrochemical industry, is selected to simulate the proposed reactor concept.

2. Model development

2.1. Description of the microstructured membrane reactor (MMR) concept

A schematic illustration of the reactor concept is shown in Figure 1. The reactor consists of N connected micro packed beds, each having its own heat exchange unit. To achieve this the reactor could be produced from a tubular dense membrane, for example a ceramic perovskite such as $\text{Ba}_{0.5}\text{Sr}_{0.5}\text{Co}_{0.8}\text{Fe}_{0.2}\text{O}_{3-\delta}$ (BSCF), characterised by high oxygen permeation flux and good thermal and mechanical stability [30]. In this study we use such a membrane as an example of the possible implementation. The membrane is placed inside a tube that forms the reactor wall. The annulus

between the membrane and the reactor shell is packed with catalyst particles, and surrounding the reactor wall is the coolant channel. The coolant channel is divided into several zones, with independent temperatures along the length of the reactor. The hydrocarbon and an inert gas are fed to the annular packed bed, while oxygen is fed to the membrane side; oxygen permeates into the packed bed and the rate of oxygen transfer may be controlled by structuring the membrane along the length of the reactor.

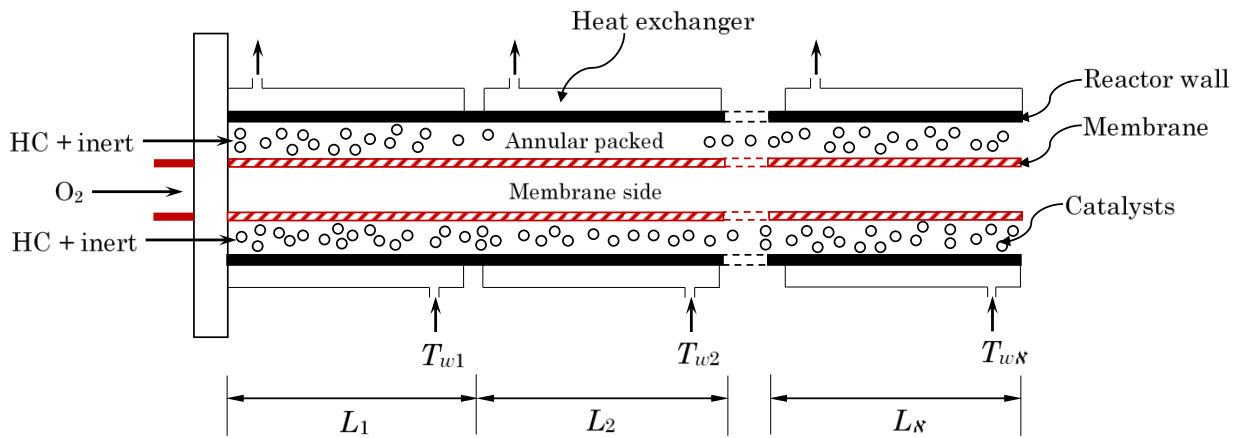


Figure 1. Schematic of the microstructured membrane reactor (MMR) concept.

2.2. Reactor modelling

Figure 2 shows a cross-section of the reactor with the relevant dimensions indicated. A one-dimensional pseudo-homogeneous model of the reactor is developed based on the following assumptions:

- Ideal gas behaviour.
- Uniform and fully developed laminar velocity profile with negligible pressure drop.
- Thin active catalyst layer (100 μm), hence internal heat and mass transfer resistances are negligible and catalyst efficiency, $\eta = 1$ [31,32].
- Radial concentration and temperature gradients are negligible.

- No axial dispersion.
- Chemical reactions take place only in the packed channel.

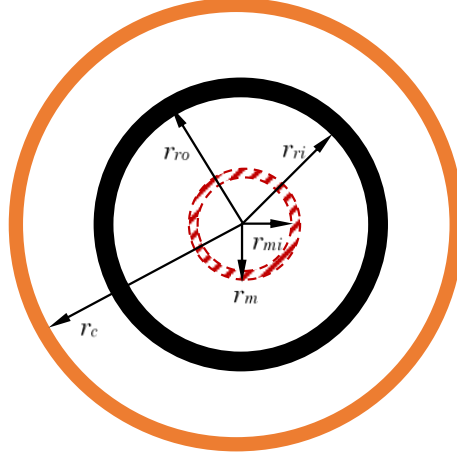


Figure 2. Sectional view of MMR showing relevant dimensions.

Following the approach adopted by Dixon [33], the steady-state mass balance for specie i can be written as shown in Eqs. (1) and (2).

Reaction side:

$$\frac{dF_i}{dz} = \pi(r_{ri}^2 - r_{mo}^2)\rho_B \sum_J^N \nu_{i,j} r_{i,j} + 2\pi r_{mi} J_i \quad (1)$$

Distributed gas side:

$$\frac{dF_i^d}{dz} = -2\pi r_{mi} J_i \quad (2)$$

where $i = \{oX, TA, P, PA, CO_x, O_2, H_2O, N_2\}$ and $\rho_B = \rho_{cat}(1 - \varepsilon_B)$.

The energy equation accounts for the heat of reaction, transport of enthalpy by diffusing species and conduction by the membrane itself, as well as heat exchange between the reaction side and the coolant. The balances are given in Eqs. (3) and (4).

Reaction side:

$$\sum F_i C_{p,i} \frac{dT}{dz} = \pi(r_{ri}^2 - r_{mo}^2) \rho_B \sum_j^N r_j (-\Delta H_{r,j}) + 2\pi r_{mi} [J_i C_{p,i} + U_m] (T^d - T) + 2\pi r_{ri} U (T_w - T) \quad (3)$$

Distributed gas side:

$$\sum F_i^d C_{p,i} \frac{dT^d}{dz} = 2\pi r_{m,i} U_m (T - T^d) \quad (4)$$

The model equations represent an initial value problem with the following boundary conditions:

$$F_i(z=0) = F_{i,in} ; T(z=0) = T_{in} \quad (5)$$

$$F_i^d(z=0) = F_{i,in}^d ; T^d(z=0) = T_{in} \quad (6)$$

In the equations above, J_i is the permeation flux of specie i through the membrane. $J_{i \neq O_2} = 0$ as dense perovskite membranes have been shown to exhibit infinite oxygen permselectivity [34,35].

The overall heat transfer coefficient between the distributed gas side and the reaction side U_m and that between the reaction channel and the heat transfer medium U are estimated using the concept of thermal resistances in series, Eq. (7).

$$\frac{1}{U_m} = \frac{1}{h_{gm}} + \frac{r_{mi} \ln(r_{mo}/r_{mi})}{\lambda_m} + \frac{1}{h_{gw}} \quad (7a)$$

$$\frac{1}{U} = \frac{1}{h_{gw}} + \frac{r_{ri} \ln(r_{ro}/r_{ri})}{\lambda_r} + \frac{r_{ri}}{(r_c - r_{ro})} \frac{1}{h_{wc}} \quad (7b)$$

The heat transfer coefficient from gas to inside of membrane h_{gm} is estimated from Nusselt number correlation for fully developed laminar flow in a circular cross-section with constant wall temperature, given by Shah and London [36], Eq. (8).

$$Nu = h_{gm} d_{m,i} / \lambda_m = 3.657 \quad (8)$$

Heat transfer coefficient from bulk gas to the reactor wall, h_{gw} , calculated from the following correlation proposed by Specchia *et al.* [37], Eq. (9).

$$h_{gw} = h_{w,0} + h_{w,conv} \quad (9)$$

$h_{w,0}$ and $h_{w,conv}$ are the stagnant and convective contributions, respectively, given in Eq. (10).

$$\frac{h_{w,0} d_p}{\lambda_g} = 2\varepsilon_b + \frac{1 - \varepsilon_B}{0.0024 \left(\frac{d_{ri}}{d_p} \right)^{1.58} + \frac{1}{3} \left(\frac{\lambda_g}{\lambda_p} \right)} \quad (10a)$$

$$\frac{h_{w,conv} d_p}{\lambda_g} = 0.0835 Re_p^{0.91} \text{ for } 10 \leq Re_p \leq 1200 \quad (10b)$$

$$\text{where } Re_p = \rho_g u d_p / \mu$$

The convective heat transfer coefficient from the reactor wall to the coolant, h_{wc} , estimated from the following relations [38]:

$$h_{wc} d_{H,c} / \lambda_c = (Nu_1^{1/3} + Nu_2^{2/3})^{1/3} \quad (11)$$

where:

$$Nu_1 = 3.657 + 1.22 \left(\frac{d_{ro}}{d_c} \right)^{-0.5} \quad (12a)$$

$$Nu_2 = 1.615 \left[1 + 0.14 \left(\frac{d_{ro}}{d_c} \right)^{-0.5} \right] \left(Re Pr \frac{d_{H,c}}{L} \right)^{1/3} \quad (12b)$$

$$Re = \rho_c u_c d_{H,c} / \mu_c \text{ and } Pr = C_{pc} \mu_c / \lambda_c \quad (12c)$$

For comparison of performance of different reactors, we use simulations of a microstructured reactor and a conventional fixed bed reactor (FBR), both operating under co-feed mode and cooled by a molten salt. For the co-feed configurations, Eqs. (1) and (3) apply with the terms involving the permeation fluxes reducing to zero, giving the standard one-dimensional plug flow equations, Eqs. (13) - (14).

$$\frac{dF_i}{dz} = \pi(r_{ri}^2 - r_{mo}^2) \rho_B \sum_j^N v_i r_{i,j} \quad (13)$$

$$\sum F_i C_{p,i} \frac{dT}{dz} = \pi(r_{ri}^2 - r_{mo}^2) \rho_B \sum_j^N r_j (-\Delta H_{r,j}) + 2\pi r_{ri} U (T_w - T) \quad (14)$$

2.3. Axial distribution of oxygen feed and coolant temperature

Two different reactor arrangements are investigated in order to find the optimum means of introducing oxygen into the reactor, as shown in Figure 3. First, a uniform oxygen distribution is considered, where the oxygen flux is constant over the reactor length, $J_{O_2} = \text{const.}$, Figure 3(a). In this case the membrane is assumed to have constant thickness along the length of the reactor, and hence a uniform resistance to oxygen permeation.

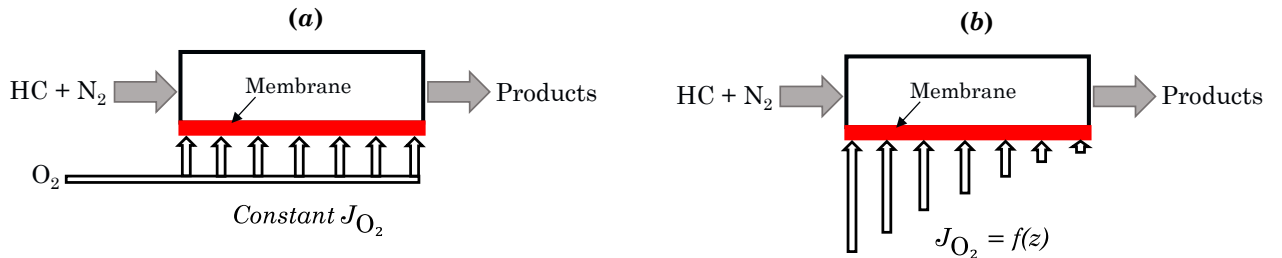


Figure 3. Schematic of the oxygen permeation profiles in the MMR.

(a) A uniform oxygen permeation profile, (b) A variable oxygen permeation profile.

An alternative approach is non-uniform dosing, where the largest amount of oxygen is permeated near the reactor inlet, which then decreases steadily along the reactor length, $J_{O_2} = f(z)$, as shown in Figure 3(b), similar to the concept investigated by Hüpmeier *et al.* [39, 40]. To realise this in practice the membrane surface may be treated to attenuate its thickness to increase the resistance to oxygen permeation along the reactor length. The axial linear oxygen dosing profile can be described by:

$$J_{O_2}(z) = \zeta z + c \quad (15)$$

where ζ is $(J_{O_2(z=L)} - J_{O_2(z=0)})/L$ and c is $J_{O_2(z=0)}$.

The \aleph heat exchange zones surrounding the reactor provide a stage-wise temperature distribution across the length of the reactor, which can be represented by the following piecewise function:

$$T_{w,n}(z) = \begin{cases} T_{w,1} & 0 < z \leq L_1 \\ T_{w,2} & L_1 < z \leq L_2 \\ T_{w,3} & L_2 < z \leq L_3 \\ \vdots & \vdots \\ T_{w,(\aleph-1)} & L_{(\aleph-2)} < z \leq L_{(\aleph-1)} \\ T_{w,\aleph} & L_{(\aleph-1)} < z \leq L_{\aleph} \end{cases} \quad (16)$$

where $n = 1, 2, \dots, \aleph$; $T_{w,n}$ is temperature at n th zone, and $L_n = L/\aleph$ is the length of a zone.

2.4. Reaction case study and kinetics

The selective oxidation of *o*-xylene in the gas-phase over V_2O_5/TiO_2 catalyst was selected to simulate the proposed reactor design. The kinetics and mechanism of this reaction has been the

subject of extensive study [41–43]. The reaction is fast, strongly exothermic and is typically carried out in a fixed bed reactor at near atmospheric pressure, temperature range of 300–450°C and *o*-xylene feed concentration between 0.5 and 1.8 mol% to stay outside of the flammability limits [44]. Mechanistically, the reaction proceeds by several parallel and consecutive steps involving *o*-tolualdehyde and phthalide as the main intermediates with carbon oxides as total oxidation products and maleic anhydride (MA) as by-product.

Modern industrial vanadium-titanium oxide catalysts for *o*-xylene oxidation, such as the Süd-Chemie PHTHALIMAX[®], consisting of multiple layers modified with antimony oxide (Sb₂O₃) and small amount of alkali metal ions, e.g. caesium or niobium, as promoters for optimised activity and selectivity have been developed [45,46]. These state-of-the-art catalysts allow PA selectivity of 78-82% to be achieved. However, to the best of our knowledge no relevant kinetic data based on these catalytic systems currently exist in the open literature.

For this present work, the reaction network given in Figure 4 and the kinetic model proposed by Papageorgiou and Froment [31,47] based on the conventional V₂O₅/TiO₂ catalyst was employed. The kinetic model accounts in detail for the interaction of the reacting species with the reduced and the oxidised active sites of the catalyst, and incorporates the influence of oxygen partial pressure on the reaction rates.

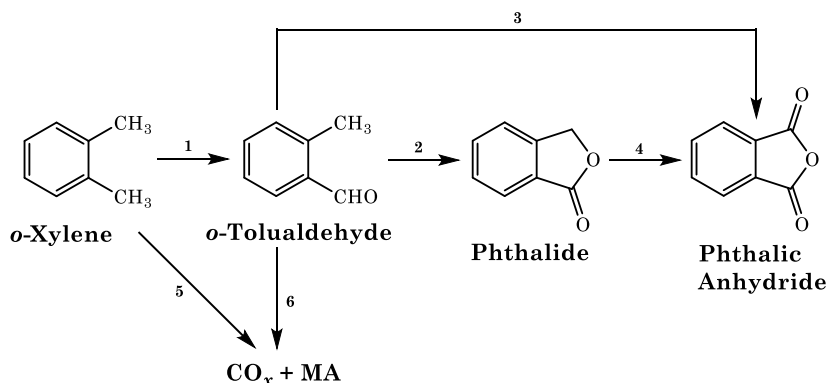


Figure 4. Reaction network for the selective oxidation of *o*-xylene to PA [31,47].

The rates of consumption of *o*-xylene and of the formation of products are given by:

$$r_{oX} = \frac{(k_1 + k_5)p_{oX}p_{O_2}}{DEN} \quad (17)$$

$$r_{TA} = \frac{k_1p_{oX}p_{O_2} - p_T[k_2p_{O_2}^{0.5} + (k_3 + k_6)p_{O_2}]}{DEN} \quad (18)$$

$$r_{PH} = \frac{(k_2p_T - k_4p_P)p_{O_2}^{0.5}}{DEN} \quad (19)$$

$$r_{PA} = \frac{k_3p_Tp_{O_2} + k_4p_Pp_{O_2}^{0.5}}{DEN} \quad (20)$$

$$r_C = \frac{(k_5p_{oX} + k_6p_T)p_{O_2}}{DEN} \quad (21)$$

where $DEN = [1 + K_o p_{O_2}^{0.5} + K_A (p_{oX} + p_T) p_{O_2}^{0.5} + K_B (p_T + p_P + p_{PA})]^2$ and C is the by-products (CO, CO₂ and MA).

The rate constants and adsorption equilibrium constants are expressed by Arrhenius type equations, Eqs. (22) and (23), and the kinetic parameters are given in Table 1.

$$k_j = A_{o,j} \exp(-E_{a,j} / RT) \quad (22)$$

$$K_a = A_a \exp(-\Delta H_a / RT) \quad (23)$$

Table 1. Kinetic and thermodynamic parameters for the catalytic oxidation of *o*-xylene [31].

Reaction (<i>j</i>)	$A_{o,j}$	$E_{a,j}$	$-\Delta H_{r,j}$
	(mol kg _{cat} ⁻¹ s ⁻¹ atm ^{-1.5}) / (mol kg _{cat} ⁻¹ s ⁻¹ atm ⁻²)	(kJ mol ⁻¹)	(kJ mol ⁻¹)
1	5.020×10 ⁷	84.75	3.27×10 ²
2	2.188×10 ⁴	42.46	3.08×10 ²
3	1.906×10 ³	23.79	6.27×10 ²
4	3.101×10 ⁶	66.13	3.19×10 ²
5	4.090×10 ⁹	114.9	32.5×10 ²
6	1.830×10 ⁶	69.16	32.5×10 ²
Adsorption constants	A_a	$-\Delta H_a$ (kJ mol ⁻¹)	
K_o (atm ^{-0.5})	2.280	3.567	
K_A (atm ⁻¹)	15.858	21.82	
K_B (atm ⁻¹)	0.419	39.07	

2.5. Numerical simulation and optimization of reactor model

The system of coupled ordinary differential equations (ODE) with the initial conditions is solved using the ODE-solver ode113, implemented in MATLAB R2016b. Variations in physical properties of the gas, such as density, specific heat, thermal conductivity, with temperature and composition along the reaction channel were taken into consideration, while physical properties of the catalyst, reactor wall, membrane, and coolant were assumed to be constant. A summary of the simulation parameters for the microstructured reactor is given in Table 2. A conventional fixed

bed reactor operating under typical industrial conditions for PA synthesis was also simulated using the data in Papageorgiou and Froment [31].

Table 2. Parameters for simulation of the microstructured membrane reactor.

Reactor		
Length	L	0.3 m
Membrane outer diameter	d_{mo}	3 mm
Membrane thickness	δ_m	50 μm
Inner diameter of reactor tube	d_{ri}	5 mm
Reactor tube thickness	δ_r	0.3 mm
Thermal conductivity of reactor material	λ_r	15 $\text{W m}^{-1} \text{K}^{-1}$
Thermal conductivity of membrane	λ_m	0.3 $\text{W m}^{-1} \text{K}^{-1}$
Total inlet volume flowrate	Q_T	50 mL min^{-1}
Catalyst		
Catalyst particle size	d_p	250 μm
Catalyst density	ρ_{cat}	2138 $\text{kg}_{cat} \text{m}_{cat}^{-3}$
Bed porosity	ε_B	0.40

Optimization was performed on the reactor model using MATLAB's genetic algorithm (*GA*) to determine optimum conditions in the reactor that will maximise PA selectivity at the reactor outlet. The genetic algorithm specifies the optimization variables, Ω , calls an external integrator to solve the ODE equations for each segment of the reactor and finally computes the value of the objective function, defined in Eq. (24)

$$\max_{\Omega} \frac{F_{PA,out}}{F_{oX,in} - F_{oX,out}} \quad (24)$$

s.t.

$$\Omega_{\min} \leq \Omega \leq \Omega_{\max} \quad (25)$$

where Ω is a vector of control variables with $\aleph+5$ elements, defined as in Eq. (26), \aleph being the total number of heat exchange sections along the length of the reactor.

$$\Omega = [T_{w,1} \quad \cdots \quad T_{w,n} \quad \cdots \quad T_{w,\aleph} \quad T_{in} \quad J_{O_2} \quad y_{oX,in} \quad y_{O_2,in} \quad P] \quad (26)$$

The GA starts by randomly generating a number of points, which is called the initial population. A new population is generated at each iteration by mutation, crossover and selection from the current population, based on the fitness value of each point, that is the value of the objective function in the optimization problem. The new population of candidate solutions is then used for the next iteration of the algorithm, so that over successive generations, the GA repeatedly improves a population of individual solutions, which evolves towards the optimal solution [48]. The GA algorithm was particularly suited to this problem because the derivative-free optimization method was easy to implement and could utilise the advanced MATLAB integrator. In this work, the population size at each generation and the maximum number of generations used for the GA optimization were both set to 200 in order to obtain the optimal global solution. The algorithm stops the iterative process when the stopping criteria for the optimization is met, that is when the maximum number of generations is exceeded.

Thus, the aim of the optimization was to find the best combination of the cooling jacket temperature in each section along the length of the reactor, the feed temperature, oxygen permeation flux through the membrane, concentrations of *o*-xylene and oxygen at the catalyst tube

inlet as well as the total reactor pressure. The limits of the operating parameters in Ω in terms of the range of permissible changes for the numerical optimization are given in Table 3.

Table 3. Bounds of operating variables for numerical optimization.

Variable name		Lower bound	Upper bound
		(Ω_{\min})	(Ω_{\max})
Coolant temperature in section n (°C)	$T_{w,n}$	300	400
Inlet temperature (°C)	T_{in}	300	400
Oxygen permeation flux (mol m ⁻² s ⁻¹)	J_{O_2}	0	0.1
Inlet concentration of <i>o</i> -xylene (mol%)	$y_{oX,in}$	1.0	1.5
Inlet concentration of oxygen (mol%)	$y_{O_2,in}$	5.0	21.0
Reactor operating pressure (bar)	P	1.0	1.3

The reactor performance was evaluated in terms of conversion, selectivity and yield, defined respectively as shown in Eq. (27).

$$X_{oX} = (F_{oX,in} - F_{oX}) / F_{oX,in} \quad (27a)$$

$$S_{PA} = F_{PA} / (F_{oX,in} - F_{oX}) \quad (27b)$$

$$Y_{PA} = X_{oX} S_{PA} \quad (27c)$$

3. Results and discussion

3.1. Simulation of a conventional fixed bed reactor (FBR)

As a base case for validation of the model and the numerical techniques used to solve it, a conventional FBR operating under typical industrial conditions with *o*-xylene and air fed at the reactor inlet was simulated using Eqs. (13) and (14). Simulation data for the FBR were based on parameters from Papageorgiou and Froment [31] and are given in Table 4.

Table 4. Simulation data for FBR.

T_{in}, T_w	360°C
y_{oX}	1 mol%
p_{O_2}	0.21 atm
P	1.2 atm
G	1.3 kg m ⁻² s ⁻¹
L	3 m
d_p	4.3 mm
d_r	25.4 mm

Results in Figure 5 show that conversion of *o*-xylene takes place from the inlet to the outlet of the reactor. Since *o*-tolualdehyde and phthalide are intermediates, their concentrations reach a maximum at relatively low conversions of *o*-xylene and thereafter decreases with the reactor length. Furthermore, the maximum concentration of *o*-tolualdehyde is greater than that of phthalide, indicating that the former is the first intermediate in the reaction sequence. At almost full conversion of *o*-xylene, the selectivity to phthalic anhydride and by-products are 70% and ~30%, respectively. The results obtained from this simulation are in good agreement with several experimental observations on catalytic oxidation of *o*-xylene [32,42,47]. Figure 5 also shows the

axial temperature profile in the reactor, where it can be seen that a hot spot with a ΔT_{max} of 20.2° is formed near the reactor inlet, which drops sharply with the reactor length. The non-uniform temperature profile can be attributed to high exothermicity of the reaction as well as the ineffective heat transfer in the catalyst bed. The position and size of the hot spot temperature in the FBR agrees well with the results reported by Papageorgiou and Froment [31].

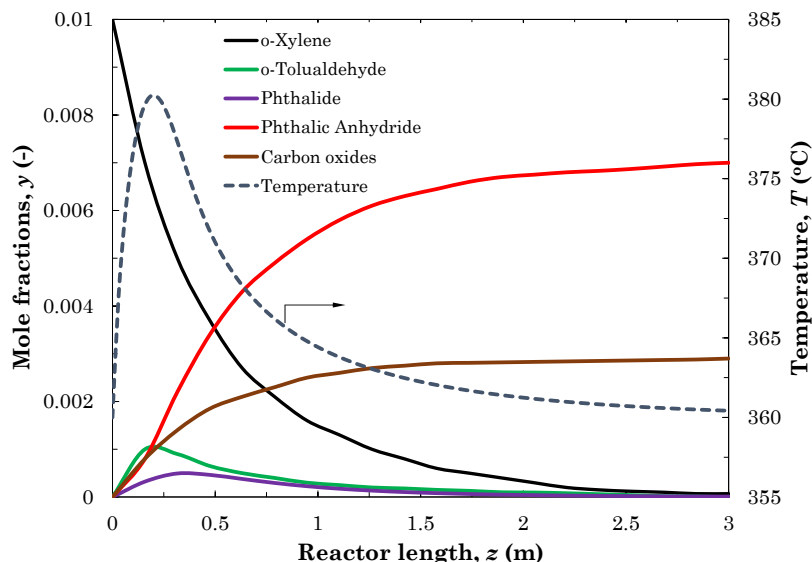


Figure 5. Axial concentration and temperature profiles in FBR.

3.2. Co-feed microstructured vs fixed bed reactors

Here, a co-feed microstructured reactor (CMR), operating under similar o -xylene and oxygen feed concentrations as well as inlet and coolant temperatures as the conventional FBR was simulated. Figure 6 shows the temperature profile and selectivity–conversion plot for the FBR and CMR configurations. It can be observed from Figure 6(a) that the CMR demonstrates a significant reduction in the temperature gradient with a ΔT_{max} of 1.5° compared to a hot spot temperature of $\Delta T = 20.2^\circ$ in the FBR. Figure 6(b) shows that the CMR gives a slightly higher PA selectivity of 72% compared to 70% for the FBR at full conversion of o -xylene. These results may be attributed to the enhanced heat transfer characteristics of the microstructured reactor, giving a near-

isothermal profile. The lower temperature gradient in the CMR thus favours higher PA selectivity by suppression of the total oxidation of *o*-xylene into carbon oxides and maleic anhydride. The ability of microstructured reactors to improve selectivity in highly exothermic selective oxidation reactions for the synthesis of anhydrides has been demonstrated in other studies [24,49].

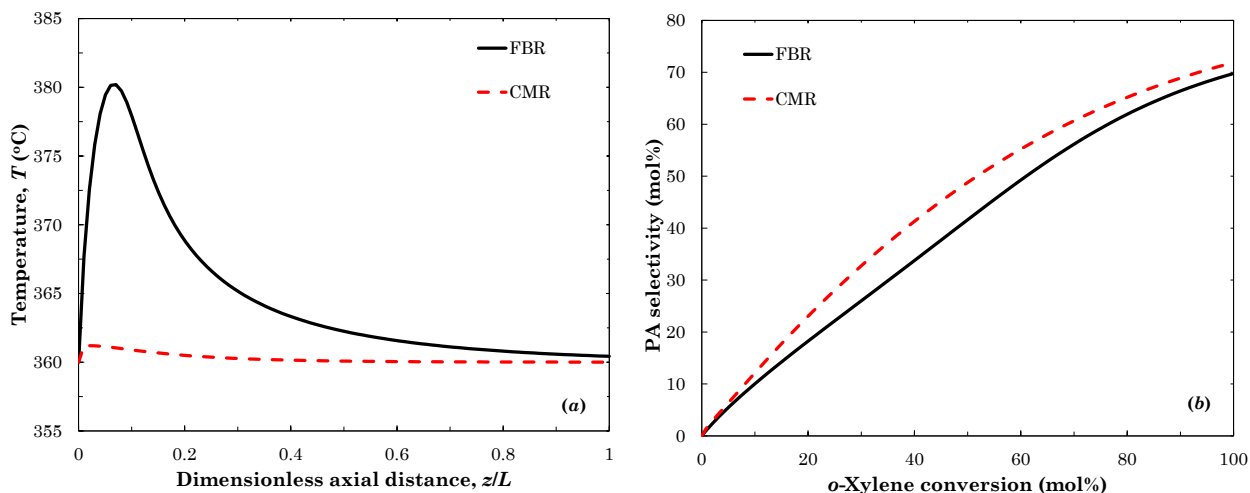


Figure 6. Simulation results for CMR and FBR. (a) Axial temperature profile, (b) selectivity-conversion plot. Feed contains 1 mol% *o*-xylene and 21 mol% oxygen. $T_{in} = T_w = 360^\circ\text{C}$.

3.3. Microstructured membrane reactor with a constant wall temperature

In the microstructured membrane reactor (MMR) configuration, *o*-xylene and nitrogen premixed with a small amount of oxygen are introduced at the annular packed bed inlet, while the rest of oxygen is fed through the membrane side. In this case, the reactor is considered to have one heat exchange section with a single cooling jacket temperature. Residence time in the reactor is defined as a ratio of the volume of the annular space filled with catalyst to the total inlet volumetric flow rates, $Q_m + Q_r$, hence permitting direct comparison with the CMR. 3D surface plots in Figure 7 show the effects of wall temperature and oxygen permeation flux over the range considered in the simulation on *o*-xylene conversion and PA selectivity for the uniformly permeated MMR configuration presented in Figure 3(a).

It can be seen from Figure 7 that *o*-xylene conversion increases rapidly with temperature at a given oxygen flux, reaching full conversion at temperatures between 340 and 400°C. In the region of lower temperatures, the oxygen permeation rate has a strong influence on *o*-xylene conversion. As flux increases, conversion increases up to a maximum value and then declines slightly thereafter. This is because high permeation flux strongly increases the flow rate and convective effect in the annular packed bed, thus lowering the oxygen residence time. At coolant temperatures above ~340 °C, however, oxygen permeation flux has less impact, as high conversion is achieved at all ranges of oxygen flux considered in the simulation. PA selectivity, on the other hand, increases up to a maximum and then decreases as both coolant temperature and oxygen permeation flux increase. From Figure 7, it follows that a high PA selectivity can be achieved at lower temperatures and oxygen molar fluxes. This is because higher temperature and oxygen partial pressure promote oxidation of *o*-xylene and *o*-tolualdehyde into by-products, as shown in the reaction scheme in Figure 4, thus decreasing PA selectivity. Similarly, at low oxygen partial pressures in the reactor, the degree of oxidation and activity of the catalyst are lower, so that hot spots and the associated total oxidation are reduced [50]. The optimal conversion, selectivity and yield profiles in the MMR with a constant wall temperature are plotted in Figure 8. show that maximum PA selectivity achieved in the reactor is 76.3% at a coolant temperature of 325.1°C and oxygen permeation flux of 0.0142 mol m⁻² s⁻¹. Thus, PA selectivity obtained in the MMR is significantly higher than that in the co-feed reactor configurations. The temperature profile (not shown in Figure 8) is essentially flat owing to the reaction occurring uniformly over the entire length of the reactor.

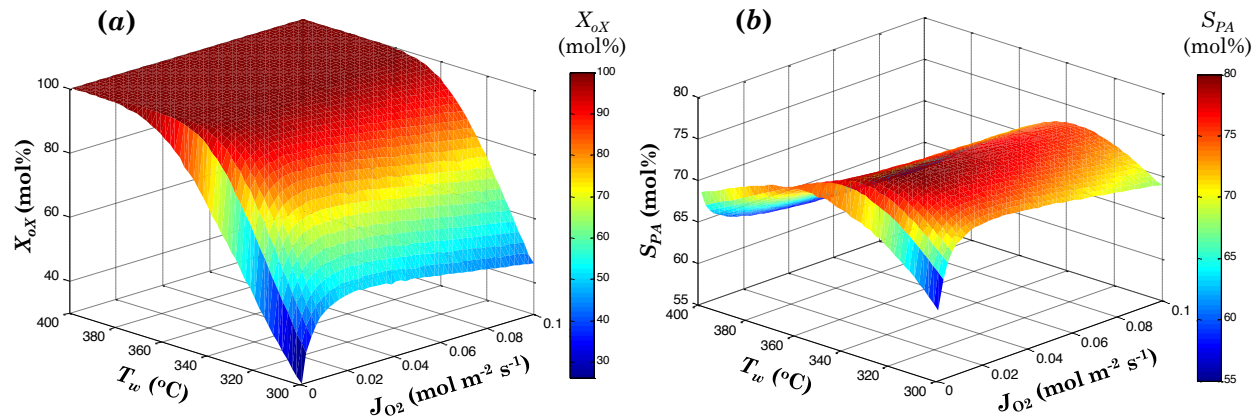


Figure 7. 3D plots of results in the MMR with a single wall temperature. Variation of: (a) *o*-xylene conversion, (b) PA selectivity, with wall temperature and oxygen permeation flux.

Total feed contains 1 mol% *o*-xylene and 21 mol% oxygen. $T_{in} = 300^\circ\text{C}$.

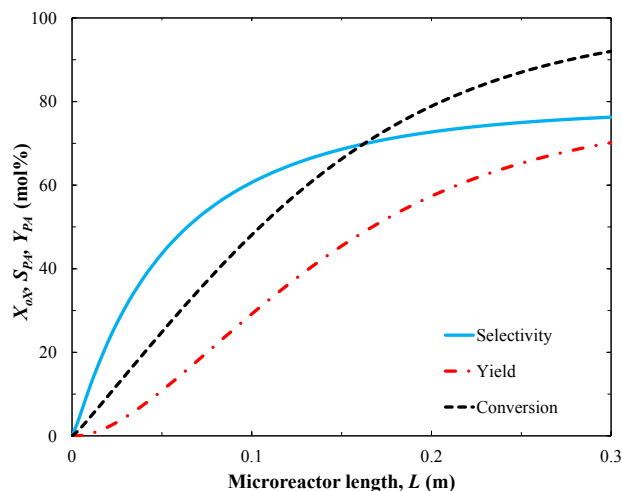


Figure 8. Optimal axial profiles in the MMR with uniform permeation and single wall temperature. Simulation parameters for the reactor are given in Table 3.

One consequence of the distributed feeding approach, as evident from Figure 8, is that *o*-xylene conversion is reduced to 91.9% compared to 100% achieved in the CMR and FBR, shown in Figure 6. This observation can be explained by the enhanced heat removal capability of the concept reactor, giving a lower average temperature and, hence, a reduced conversion compared to the

conventional FBR. The lower local oxygen concentration also contributes to the decrease in the hydrocarbon conversion. Furthermore, distributing the oxygen feed along the length of the MMR produces a distinctly different residence time distribution of the reactants compared to the CMR [51–54]. The average contact time in the membrane reactor is thus lower than in the co-feed reactor, resulting in a reduced *o*-xylene conversion for identical overall feed flow rates.

The differences in residence time behaviour of the reactants in the CMR and MMR can be explained by the following analysis. For simplicity, consider a case with no chemical reactions, Eq. (1) can be re-written as

$$\frac{dF_i}{dz} = 2\pi r_{mi} J_i \quad (28)$$

For the CMR, all the reactants are fed at the inlet with no permeation through the reactor wall, hence $J_i = 0$, and the total molar flow rate in the catalyst bed, $\sum F_i$, is constant throughout the length of the reactor. Reactants, therefore, have the same residence time, given as $\tau = V_r/Q_T$. Note that Q_T and V_r are the total volumetric flow rate of reactants entering the catalyst bed and volume of the annular space, respectively, for the CMR configuration. In the CMR, the residence time required to achieve full conversion of *o*-xylene was 4.5 s. On the other hand, for the MMR there is permeation of oxygen through the membrane into the catalyst bed, while other species are fed at the inlet. Hence, the total flow rate in the MMR can be expressed as the sum of the flow through the inlet plus that permeated through the membrane, as given by Eq. (29)

$$F_T(z) = \sum F_i + \int_0^L 2\pi r_{mi} J_{O_2}(z) dz \quad (29)$$

Thus, in the MMR, there is an increase in the total flow rate along the length of the reactor. The higher the permeation rate the greater the axial flow rate increase. Unlike the CMR, all the reactants in the MMR do not spend equal amount of time in the reactor volume. Oxygen molecules permeated into the annulus near the reactor inlet have considerably longer contact time with the catalyst bed compared to those permeated near the reactor exit, which do not have enough time to react. Hence oxygen molecules have a distribution of residence times in the MMR depending on the position where it permeates into the catalyst bed. According to Tonkovich *et al.* [53], the residence time of the reactants fed through the catalyst bed and the average residence time of the distributed oxygen in the MMR can be expressed as shown by the expressions in Eq. (30) and Eq. (31), respectively

$$\tau_r = \frac{V_r}{Q_r + 0.5Q_m} \quad (30)$$

$$\langle \tau \rangle_m = \frac{2V_r}{Q_m} \left[\frac{2(Q_r + Q_m)}{Q_m} \ln \left\{ \frac{Q_r + Q_m}{Q_r + 0.5Q_m} \right\} - 1 \right] \quad (31)$$

where Q_m and Q_r are the volumetric flow rates of the streams entering the catalyst bed and membrane inlets, respectively.

In the MMR, assuming *o*-xylene and nitrogen are fed to the catalyst bed while all the oxygen is distributed via the membrane, the residence time of the hydrocarbon plus inert was estimated from Eq. (30) to be 5.1 s while the average residence time for oxygen permeated through the membrane was estimated as 2.4 s from Eq. (31). Thus, in the MMR, the reactants fed at the inlet spend slightly more time in the reactor while the distributed oxygen has less contact time. Compared to the CMR residence time of 4.5 s, the average residence time for all reacting species and products in the MMR was 3.7 s for the same overall feed flow rate. The gain in selectivity obtained in the MMR

with a constant cooling jacket temperature thus appears to be offset by a decrease in *o*-xylene conversion as a result of the different contact time pattern as well as the lower local oxygen concentration. To achieve full conversion, either a higher coolant temperature or longer residence time may be used, but these could have detrimental effect on selectivity. The lower conversion-higher selectivity effects observed in this work are in agreement with the findings of several authors on membrane or distributed dosing reactors for partial oxidation reactions [27,33,53,55,56].

The reactor configuration with a varying oxygen permeation flux shown in Figure 3(b) was also simulated with the same parameters as for the uniformly permeated reactor discussed above. The optimum PA selectivity was found to be 76.3% with *o*-xylene conversion of 92.2%, which are quite similar to the results obtained with the uniformly dosed reactor, where oxygen flux was constant across the length of the reactor. Clearly, there was no significant differences in the optimised performance of both reactor configurations, hence subsequent simulations were carried out only with the uniformly permeated MMR.

3.4. Microstructured membrane reactor with distributed wall temperatures

In order to explore the effects of discrete wall temperatures along the MMR on conversion and selectivity, the simulation was repeated with the heat exchange section divided into \aleph zones of equal length. Again, the identical reaction conditions and overall flow rates as the CMR were used in the simulations. Results of the simulation with two, three and six sections are shown in Figure 9. There is a clear shift in reactor performance measures as the wall temperature changes from one section to another, as shown in Figure 9(a). While there is a marginal improvement in PA selectivity in going from two to six sections, there is a marked increase in *o*-xylene conversion, and hence PA yield. For the case of the MMR with three coolant sections, it can be seen from

Figure 9(a) that *o*-xylene conversion reached 97.1% compared to 91.9% achieved in the case of the MMR with a constant wall temperature, shown in Figure 8). Despite the increase in conversion, there is no detrimental effect on PA selectivity. In fact, there was a small improvement to 76.6% in the MMR with three cooling zones compared to 76.3% in the MMR with a uniform wall temperature. Furthermore, for the MMR with six temperature zones, *o*-xylene conversion and PA selectivity were 99% and 76.7%, respectively, showing even further enhancements in reactor performance as the number of heat exchange sections was doubled from three to six. The obvious implication of this finding is that maximum selectivity can be attained at full conversion by increasing the number of cooling jacket sections, thus preventing costly and energy intensive separation of the unreacted hydrocarbon for recycle.

In Figure 9(b), results of the numerical optimization show that the increasing number of coolant sections and different temperature zones from the inlet to the exit of the reactor gives the best performance. As the number of heat exchange sections is increased, there is no significant difference in the operating temperature at the zone next to the inlet, that is 319.8 and 316.6°C for two and six sections, respectively. However, in the intermediate and final sections the effect of staging of coolant temperatures along the length of the reactor can be clearly seen. In the last sections, the wall temperatures increase significantly with the increasing number of segments: 336.6 and 365.4°C for two and six stages, respectively. This effect gives the improved conversion and yield observed in Figure 9(a). The nature of the optimal temperature profile in the MMR is opposite to that of the conventional FBR, where the temperature of the catalyst bed near the inlet is too high, causing hot spot and loss of selectivity. These simulation results are in good agreement with the work of Anastasov and Nikolov [57] on the optimal policy of the application of a dual salt-bath to a fixed bed reactor for the selective oxidation of *o*-xylene.

Figure 10 shows the variations of the optimal coolant temperature averaged over the entire reactor length, oxygen permeation flux through the membrane and PA yield with the number of cooling jacket sections. As the number of coolant sections increased from one to six, the average wall temperature increased from 325.1 to 332.5°C with a corresponding decrease in the oxygen permeation flux from 0.0142 to 0.0124 mol m⁻² s⁻¹, as shown in Figure 10(a). These effects give further improvement in *o*-xylene conversion without loss of selectivity, leading to enhanced PA yield of about 6%, as shown in Figure 10(b). Thus, with more cooling sections, the increase in the average reactor temperature to give higher conversion is compensated for by a reduction in oxygen flux, and hence local oxygen concentration, which helps to maintain selectivity at the optimum level.

Thus, while oxygen distribution improves process selectivity but lowers conversion in the MMR with a single wall temperature, implementation of temperature distribution on the same reactor enhances conversion without loss of selectivity. The overall effect is that for the MMR with six coolant sections, PA yield of 75.9% was attained compared to 70% achieved in the conventional FBR for the similar levels of conversion of *o*-xylene.

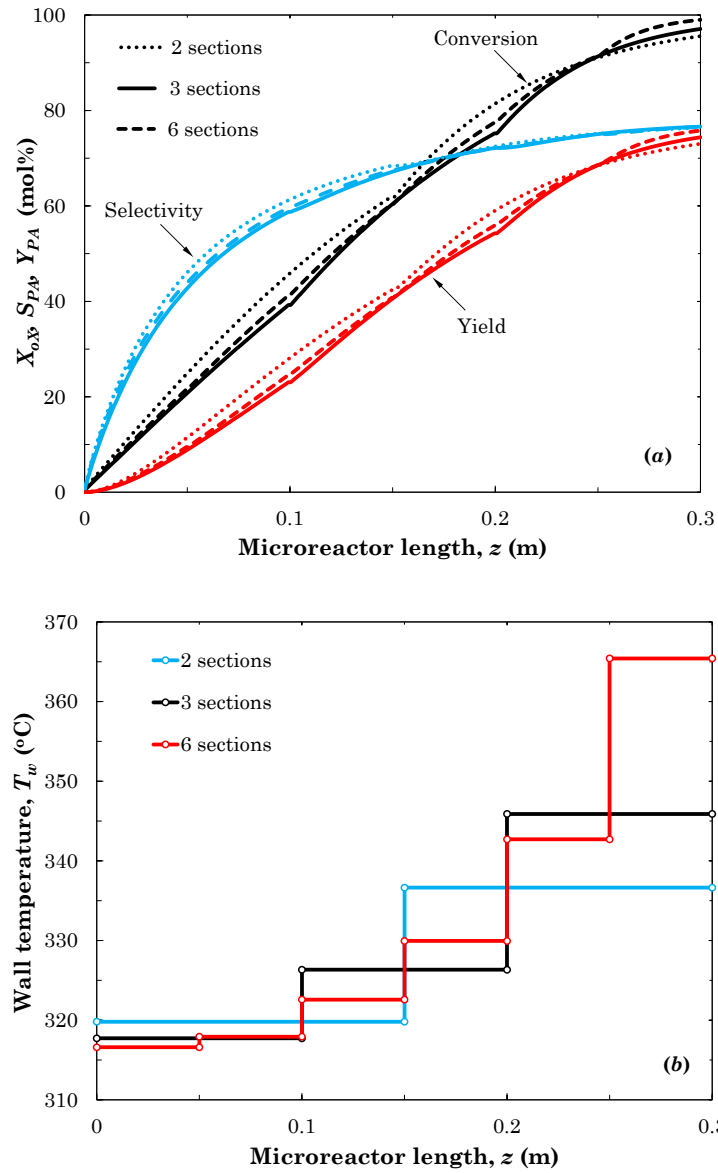


Figure 9. Optimal results in the MMR with structured wall temperatures. (a) Reactor performance measures, (b) cooling jacket temperature profiles.

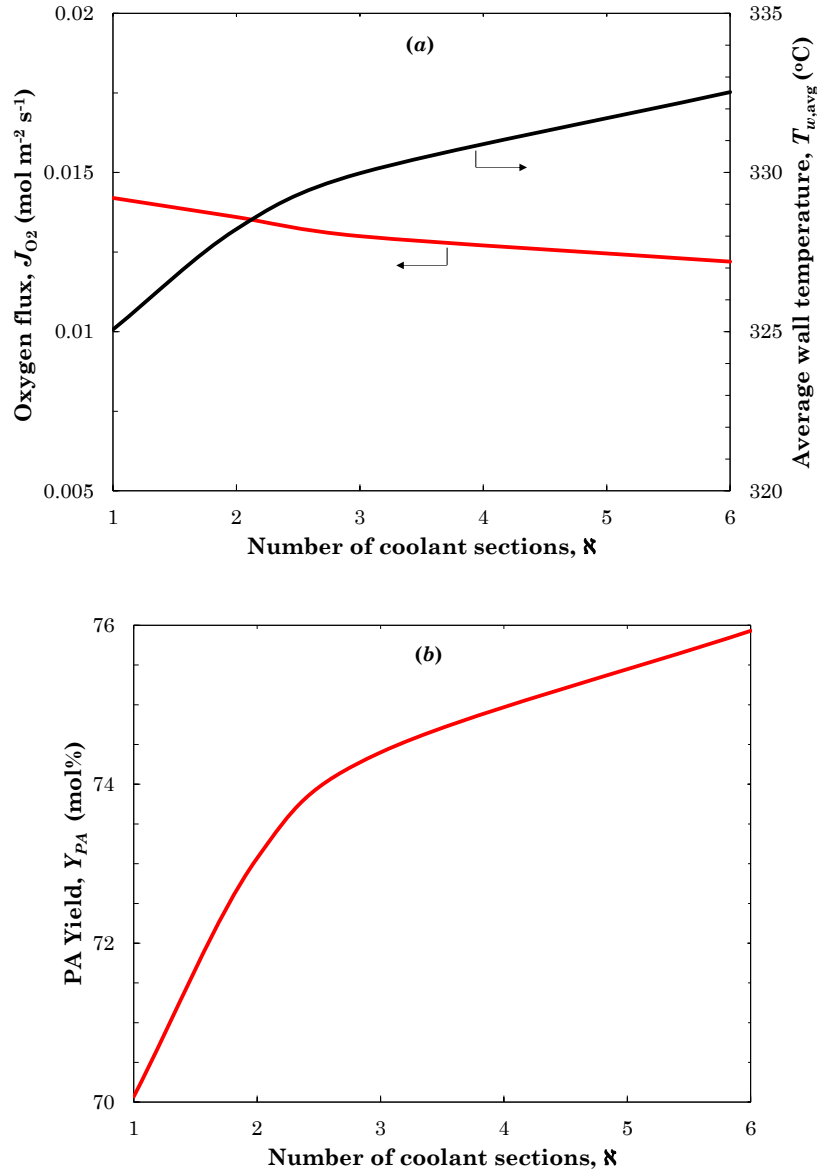


Figure 10. Effect of the number coolant sections on optimal reactor performance. (a) Optimum wall temperature and oxygen permeation flux, (b) Maximum PA yield.

Sensitivity analysis was performed on the optimization to test the response of the objective function to small changes in the reactor control variables. The analysis was done by perturbing the optimal value of one variable at a time by $\pm 10\%$ while keeping the other parameters constant. The results for wall temperature and oxygen permeation flux for the MMR with two cooling jacket

temperatures are shown in Figure 11. In all the cases considered in the simulations, it was observed that small variations in the wall temperatures along the length of the reactor produce a marked effect on the reactor performance.

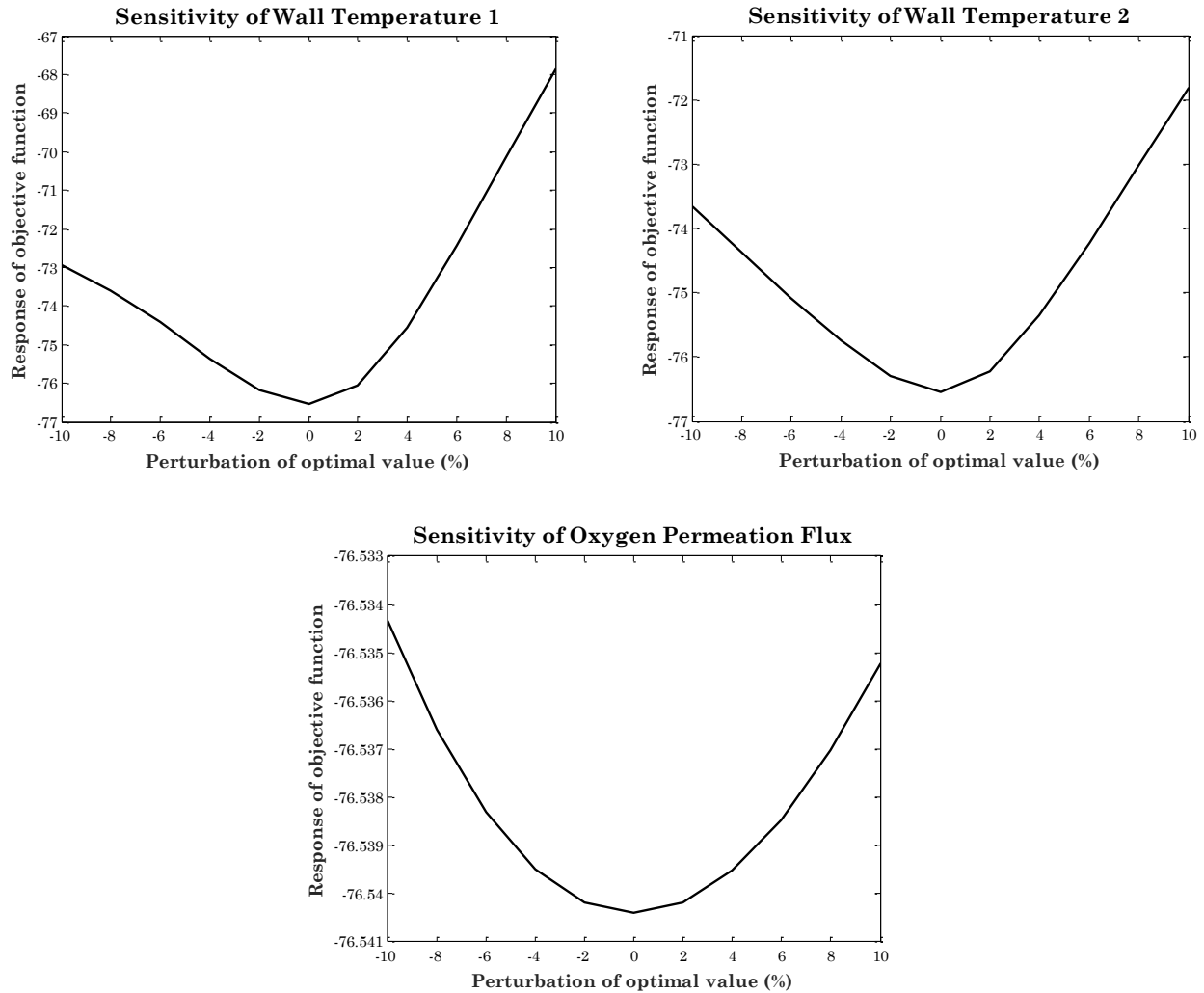


Figure 11. Response of the optimal PA selectivity to perturbations in the optimization parameters. Profiles are for the MMR with two coolant sections along the wall.

The sensitivity of the maximum PA selectivity to changes in the optimal values of other reactor parameters, including oxygen permeation flux, are less pronounced. The optimum values of other control variables in Eq. (26) are inlet temperature of 400°C, *o*-xylene and oxygen concentration in the feed to the catalyst bed of 1 mol% and 5 mol%, respectively, and total pressure of 1 atm. These

results show that the MMR configuration favours high feed temperature and a premix of ~5 mol% oxygen with the mixture of *o*-xylene and nitrogen fed to the inlet of the catalyst bed is necessary to obtain optimal results.

4. Conclusions

In this work, the principle of improving selectivity in hydrocarbon oxidation by process intensification in a novel microstructured membrane reactor concept was demonstrated by modelling and simulation. A model of the reactor concept was developed, and numerical simulation and optimization of the key operating parameters showed that by distributed feeding of oxygen and simultaneous modulation of the wall temperature along the length of the reactor, formation of the desired product can be maximised without forfeiting conversion. Thus, the concept eliminates the inherent trade-off between conversion and selectivity, which is often encountered in many hydrocarbon selective oxidations. The model was applied to the selective oxidation of *o*-xylene, the results of which showed that PA selectivity increased by 6.7% compared to a conventional fixed bed reactor for the similar level of conversion. Other significant advantages of the reactor configuration include the elimination of hot spots in the catalyst bed due to the enhanced heat transfer of the microstructured reactor, which in practice may translate into a longer catalyst lifetime and reduced thermal stress to reactor materials.

The features demonstrated by the proposed reactor concept can be extended to a wide variety of fast and highly exothermic selective oxidation reactions, where improvement in selectivity often comes with the need to lower conversion of the hydrocarbon feed to minimise formation of by-products. This configuration would be particularly useful for other selective oxidations with a network of parallel and consecutive reactions, where the kinetics and dependence of the rates of

desired and undesired reactions on oxygen concentration favour the distributed dosing of the oxygen feed [26,58,59].

It is important to mention that although a permeation equation to describe oxygen flux in the model equations would have been preferable, most of the available theoretical relations for oxygen permeation through dense perovskite membranes in the literature have parameters that are experimentally determined, typically in the 700 to 950°C temperature range, for specific types of membrane material and compositions. Since oxygen permeation in membranes is strongly dependent on temperature, extrapolating the literature data for the simulation of a reactor operating at 300–400°C in the present study would be subject to excessive error and is, therefore, not appropriate. The best approach in this case was to include oxygen permeation flux as one of the parameters to optimize. Thus, with the optimum oxygen permeation flux calculated from numerical optimization, it possible to use this value for the design and preparation of a membrane with appropriate characteristics, including thickness, permeability and stability, to practically demonstrate this process concept.

The final conclusion of this study relates to the employed method of reactor optimization. In this study, we relaxed the usually strict conditions of heat and mass fluxes along the reactor length. This situation is conceptually close to the idea of identifying the optimal state variables trajectory [60], although in our case the complete reactor system was taken as a functional module. This then allowed ‘free’ optimization of the mass and energy fluxes that resulted in innovative reactor configurations, which, arguably, cannot be attained by traditional process optimization approaches.

Acknowledgements

S.M. Aworinde and A.M. Schweidtmann gratefully acknowledge scholarship awards received from Cambridge Trust and the Ernest-Solvay-Foundation, respectively. Work on this paper was enabled in part by the National Research Foundation, Prime Minister's Office, Singapore, under its CREATE programme.

Nomenclature

Latin acronyms and letters

A_o	pre-exponential factor ($\text{mol kg}_{\text{cat}}^{-1} \text{s}^{-1} \text{atm}^{-1.5}$ or $\text{mol kg}_{\text{cat}}^{-1} \text{s}^{-1} \text{atm}^{-1.5}$)
c	intercept of axial oxygen permeation function
C	products of the total oxidation of <i>o</i> -xylene (CO, CO ₂ and MA)
C_p	heat capacity of gas ($\text{J kg}^{-1} \text{K}^{-1}$)
d	diameter (m)
d_H	hydraulic diameter of channel (m)
E_a	activation energy (J mol^{-1})
F	molar flow rate (mol min^{-1})
G	superficial mass flow rate ($\text{kg m}^{-2} \text{s}^{-1}$)
h_{gm}	heat transfer coefficient from gas to membrane ($\text{W m}^{-2} \text{K}^{-1}$)
h_{gw}	heat transfer coefficient from gas to the walls ($\text{W m}^{-2} \text{K}^{-1}$)
h_{wc}	heat transfer coefficient from wall to coolant ($\text{W m}^{-2} \text{K}^{-1}$)
ΔH_r	enthalpy of reaction (kJ mol^{-1})
ΔH_a	standard enthalpy of adsorption (kJ mol^{-1})
J_i	molar flux of species <i>i</i> through the wall ($\text{mol m}^{-2} \text{s}^{-1}$)

k_j	rate constant of reaction j ($\text{mol kg}_{\text{cat}}^{-1} \text{s}^{-1}$)
K_a	adsorption equilibrium constant $\text{atm}^{-0.5}$ or atm^{-1}
L	reactor length (m)
MA	maleic anhydride
n	n th coolant section i.e. 1, 2, ..., \aleph
N	total number of reactions
\aleph	total number of coolant sections along reactor length
Nu	Nusselt number
oX	<i>o</i> -xylene
p	partial pressure of reaction specie (atm)
P	total pressure in reactor (atm)
PA	phthalic anhydride
PH	phthalide
r	radius (m)
R	gas constant ($\text{J mol}^{-1} \text{K}^{-1}$)
Re_p	particle Reynolds number
Q	volumetric flow rate (mL min^{-1})
S	PA selectivity (mol%)
TA	<i>o</i> -tolualdehyde
T	temperature ($^{\circ}\text{C}$)
U	overall heat transfer coefficient ($\text{W m}^{-2} \text{K}^{-1}$)
X	<i>o</i> -xylene conversion (mol%)
y	molar fraction

z axial coordinate (m)

Greek letters

δ thickness (m)

ε_B catalyst bed porosity

ζ parameter of Eq. (15)

η catalyst effectiveness factor

λ thermal conductivity ($\text{W m}^{-1} \text{K}^{-1}$)

μ viscosity (Pa s)

ρ_B catalyst bulk density ($\text{kg}_{\text{cat}} \text{m}^{-3}$)

τ reactor residence time (s)

Ω optimization variable

Subscripts

c coolant

cat catalyst

g gas

i reaction specie

in inlet

j reaction number

max lower bound of optimization variable

min upper bound of optimization variable

w wall (coolant)

m membrane

p	catalyst particle
r	reactor or catalyst bed
T	total
<i>Superscripts</i>	
d	membrane side

References

- [1] F. Cavani, G. Centi, C. Perego, A. Vaccari, Selectivity in catalytic oxidation: an issue or an opportunity for innovation?, *Catal. Today*. 99 (2005) 1–3.
- [2] R.A. Sheldon, R.A. van Santen, *Catalytic Oxidation: Principles and Applications*, World Scientific, Singapore, 1995.
- [3] E. Klemm, H. Döring, A. Geisselmann, S. Schirrmeister, Microstructured reactors in heterogeneous catalysis, *Chem. Eng. Technol.* 30 (2007) 1615–1621.
- [4] J.L. Dubois, Selective oxidation of hydrocarbons and the global warming problem, *Catal. Today*. 99 (2005) 5–14.
- [5] C. Batiot, B.K. Hodnett, The role of reactant and product bond energies in determining limitations to selective catalytic oxidations, *Appl. Catal. A Gen.* 137 (1996) 179–191.
- [6] F. Cavani, N. Ballarini, S. Luciani, Catalysis for society: Towards improved process efficiency in catalytic selective oxidations, *Top. Catal.* 52 (2009) 935–947.
- [7] H. Van Milligen, B. Vanderwilp, G. Wells, Enhancements in EO/EG production technology, *Hydrocarb. Process.* 96 (2017) 53–56.
- [8] B. Moghtaderi, Review of the recent chemical looping process developments for novel

- energy and fuel applications, *Energy Fuels*. 26 (2012) 15–40.
- [9] N. Ballarini, F. Cavani, A. Cericola, C. Cortelli, M. Ferrari, F. Trifirò, G. Capannelli, A. Comite, R. Catani, U. Cornaro, Supported vanadium oxide-based catalysts for the oxidehydrogenation of propane under cyclic conditions, *Catal. Today*. 91–92 (2004) 99–104.
- [10] E. Ananieva, A. Reitzmann, Direct gas-phase epoxidation of propene with nitrous oxide over modified silica supported FeO_x catalysts, *Chem. Eng. Sci.* 59 (2004) 5509–5517.
- [11] A. Ates, C. Hardacre, A. Goguet, Oxidative dehydrogenation of propane with N₂O over Fe-ZSM-5 and Fe–SiO₂: Influence of the iron species and acid sites, *Appl. Catal. A Gen.* 441–442 (2012) 30–41.
- [12] K. Weissermel, H.-J. Arpe, *Industrial Organic Chemistry*, 3rd ed., Wiley-VCH, Weinheim, 1997.
- [13] W.G. Woods, R.J. Brotherton, Oxidations of Organic Substrates in the Presence of Boron Compounds, in: R.J. Brotherton, H. Steinberg (Eds.), *Progress in Boron Chemistry*, Vol. 3, Pergamon Press, Oxford, UK, 1970: pp. 1–115.
- [14] M. Ahlquist, R.J. Nielsen, R.A. Periana, W.A. Goddard, Product protection, the key to developing high performance methane selective oxidation catalysts, *J. Am. Chem. Soc.* 131 (2009) 17110–17115.
- [15] R.A. Periana, D.J. Taube, S. Gamble, H. Taube, T. Satoh, H. Fujii, Platinum catalysts for the high-yield oxidation of methane to a methanol derivative, *Science*. 280 (1998) 560–564.

- [16] I. Hermans, E.S. Spier, U. Neuenschwander, N. Turrá, A. Baiker, Selective oxidation catalysis: Opportunities and challenges, *Top. Catal.* 52 (2009) 1162–1174.
- [17] K. Nagai, New developments in the production of methyl methacrylate, *Appl. Catal. A Gen.* 221 (2001) 367–377.
- [18] K. Suzuki, T. Yamaguchi, K. Matsushita, C. Iitsuka, J. Miura, T. Akaogi, H. Ishida, Aerobic oxidative esterification of aldehydes with alcohols by gold-nickel oxide nanoparticle catalysts with a core-shell structure, *ACS Catal.* 3 (2013) 1845–1849.
- [19] M.P. Dudukovic, Challenges and innovations in reaction engineering, *Chem. Eng. Commun.* 196 (2008) 252–266.
- [20] H.-G. Lintz, A. Reitzmann, Alternative reaction engineering concepts in partial oxidations on oxidic catalysts, *Catal. Rev.* 49 (2007) 1–32.
- [21] V. Hessel, S. Hardt, H. Löwe, *Chemical Micro Process Engineering. Fundamentals, Modelling and Reactions*, Wiley-VCH, Weinheim, 2004.
- [22] W. Ehrfeld, V. Hessel, H. Löwe, *Micromixers: New Technology for Modern Chemistry*, Wiley-VCH, Mainz, 2000.
- [23] T.A. Nijhuis, J. Chen, S.M.A. Kriescher, J.C. Schouten, The direct epoxidation of propene in the explosive regime in a microreactor-A study into the reaction kinetics, *Ind. Eng. Chem. Res.* 49 (2010) 10479–10485.
- [24] R. Guettel, T. Turek, Assessment of micro-structured fixed-bed reactors for highly exothermic gas-phase reactions, *Chem. Eng. Sci.* 65 (2010) 1644–1654.
- [25] D.V. Bavykin, A.A. Lapkin, S.T. Kolaczkowski, P.K. Plucinski, Selective oxidation of

- alcohols in a continuous multifunctional reactor: Ruthenium oxide catalysed oxidation of benzyl alcohol, *Appl. Catal. A Gen.* 288 (2005) 175–184.
- [26] S. Thomas, C. Hamel, A. Siedel-Morgenstern, Basic Problems of Chemical Reaction Engineering and Potential Membrane Reactors, in: A. Siedel-Morgenstern (Ed.), *Membrane Reactors: Distributing Reactants to Improve Selectivity and Yield*, Wiley-VCH Verlag GmbH & Co. KGaA, Weinheim, 2010: pp. 1–27.
- [27] A. Tota, C. Hamel, S. Thomas, M. Joshi, F. Klose, A. Seidel-Morgenstern, Theoretical and experimental investigation of concentration and contact time effects in membrane reactors, *Chem. Eng. Res. Des.* 82 (2004) 236–244.
- [28] F. Klose, T. Wolff, S. Thomas, A. Seidel-Morgenstern, Operation modes of packed-bed membrane reactors in the catalytic oxidation of hydrocarbons, *Appl. Catal. A Gen.* 257 (2004) 193–199.
- [29] L. Bortolotto, R. Dittmeyer, Direct hydroxylation of benzene to phenol in a novel microstructured membrane reactor with distributed dosing of hydrogen and oxygen, *Sep. Purif. Technol.* 73 (2010) 51–58.
- [30] S. Baumann, J.M. Serra, M.P. Lobera, S. Escolastico, F. Schulze-Küppers, W.A. Meulenber, Ultrahigh oxygen permeation flux through supported $\text{Ba}_{0.5}\text{Sr}_{0.5}\text{Co}_{0.8}\text{Fe}_{0.2}\text{O}_{3-\delta}$ membranes, *J. Mem. Sci.* 377 (2011) 198–205.
- [31] J.N. Papageorgiou, G.F. Froment, Simulation models accounting for radial voidage profiles in fixed-bed reactors, *Chem. Eng. Sci.* 50 (1995) 3043–3056.
- [32] P.H. Calderbank, K. Chandrasekharan, C. Fumagalli, The prediction of the performance of packed-bed catalytic reactors in the air-oxidation of *o*-xylene, *Chem. Eng. Sci.* 32

- (1977) 1435–1443.
- [33] A.G. Dixon, Analysis of intermediate product yield in distributed-feed nonisothermal tubular membrane reactors, *Catal. Today*. 67 (2001) 189–203.
- [34] J. Sunarso, S. Baumann, J.M. Serra, W.A. Meulenber, S. Liu, Y.S. Lin, J.C. Diniz da Costa, Mixed ionic-electronic conducting (MIEC) ceramic-based membranes for oxygen separation, *J. Mem. Sci.* 320 (2008) 13–41.
- [35] H.J.M. Bouwmeester, A.J. Burggraaf, Dense ceramic membranes for oxygen separation, in: A.J. Burggraaf, L. Cot (Eds.), *Fundamentals of Inorganic Membrane Science and Technology*, Membrane Science and Technology Series Vol. 4, Elsevier, Amsterdam, 1996: pp. 435–528.
- [36] R.K. Shah, A.L. London, *Laminar Flow Forced Convection in Ducts: A Source Book for Compact Heat Exchanger Analytical Data*, Academic Press, New York, 1978.
- [37] V. Specchia, G. Baldi, S. Sicardi, Heat transfer in packed bed reactors with one phase flow, *Chem. Eng. Commun.* 4 (1980) 361–380.
- [38] *VDI Wärmeatlas*, 8th ed., Springer, Berlin, 1997.
- [39] J. Hüppmeier, S. Barg, M. Baune, D. Koch, G. Grathwohl, J. Thöming, Oxygen feed membranes in autothermal steam-reformers – A robust temperature control, *Fuel*. 89 (2010) 1257–1264.
- [40] J. Hüppmeier, M. Baune, J. Thöming, Interactions between reaction kinetics in ATR-reactors and transport mechanisms in functional ceramic membranes: A simulation approach, *Chem. Eng. J.* 142 (2008) 225–238.

- [41] R. Marx, H.-J. Wölk, G. Mestl, T. Turek, Reaction scheme of *o*-xylene oxidation on vanadia catalyst, *Appl. Catal. A Gen.* 398 (2011) 37–43.
- [42] V. Nikolov, D. Klissurski, A. Anastasov, Phthalic anhydride from *o*-xylene catalysis: science and engineering, *Catal. Rev. Sci. Eng.* 33 (1991) 319–374.
- [43] I.E. Wachs, R.Y. Saleh, Reaction network and kinetics of *o*-xylene oxidation to phthalic anhydride over V₂O₅/TiO₂ (anatase) catalysts, *Appl. Catal.* 31 (1987) 87–98.
- [44] P.M. Lorz, F.K. Towae, W. Enke, R. Jäckh, N. Bhargava, W. Hillesheim, Phthalic Acid and Derivatives. *Ullmann's Encyclopedia of Industrial Chemistry*, Wiley-VCH Verlag GmbH & Co. KGaA, Weinheim, 2007.
- [45] S. Altwasser, J. Zühlke, F. Rosowski, M. Kramer, Catalyst for the oxidation of *o*-xylene and/or naphthalene to phthalic anhydride, U.S. Pat. 0029214 A1 to BASF. (2012).
- [46] C. Gückel, M. Niedermeier, M. Estenfelder, Multi-layer catalyst for producing phthalic anhydride, U.S. Pat. 7,718,561 B2 to Süd-Chemie AG. (2010).
- [47] J.N. Papageorgiou, M.C. Abello, G.F. Froment, Kinetic modeling of the catalytic oxidation of *o*-xylene over an industrial V₂O₅-TiO₂ (anatase) catalyst, *Appl. Catal. A Gen.* 120 (1994) 17–43.
- [48] D.E. Goldberg, *Genetic Algorithms in Search, Optimization and Machine Learning*, Addison-Wesley Longman, Reading, MA, 1989.
- [49] T. Lange, S. Heinrich, C. Liebner, H. Hieronymus, E. Klemm, Reaction engineering investigations of the heterogeneously catalyzed partial oxidation of *o*-xylene in the explosion regime using a microfixed bed reactor, *Chem. Eng. Sci.* 69 (2012) 440–448.

- [50] J.N. Papageorgiou, G.F. Froment, Phthalic anhydride synthesis. reactor optimization aspects, *Chem. Eng. Sci.* 51 (1996) 2091–2098.
- [51] F. Klose, T. Wolff, S. Thomas, A. Seidel-Morgenstern, Concentration and residence time effects in packed bed membrane reactors, *Catal. Today.* 82 (2003) 25–40.
- [52] M.A. Peña, D.M. Carr, K.L. Yeung, A. Varma, Ethylene epoxidation in a catalytic packed- bed membrane reactor, *Chem. Eng. Sci.* 53 (1998) 3821–3834.
- [53] A.L.Y. Tonkovich, J.L. Zilka, D.M. Jimenez, G.L. Roberts, J.L. Cox, Experimental investigations of inorganic membrane reactors: A distributed feed approach for partial oxidation reactions, *Chem. Eng. Sci.* 51 (1996) 789–806.
- [54] A.L.Y. Tonkovich, D.M. Jimenez, J.L. Zilka, G.L. Roberts, Inorganic membrane reactors for the oxidative coupling of methane, *Chem. Eng. Sci.* 51 (1996) 3051–3056.
- [55] M. Menéndez, Membrane Reactors as Tools for Catalytic Oxidation Processes, in: D. Duprez, F. Cavani (Eds.), *Handbook of Advanced Methods and Processes in Oxidation Catalysis: From Laboratory to Industry*, Imperial College Press, London, 2014: pp. 921–942.
- [56] Y. Lu, A.G. Dixon, W.R. Moser, Y.H. Ma, Oxidative coupling of methane in a modified γ -alumina membrane reactor, *Chem. Eng. Sci.* 55 (2000) 4901–4912.
- [57] A.I. Anastasov, V.A. Nikolov, Optimal policies of operation of a fixed-bed reactor for oxidation of o-xylene into phthalic anhydride, *Ind. Eng. Chem. Res.* 37 (1998) 3424–3433.
- [58] Y. Lu, A.G. Dixon, W.R. Moser, Y.H. Ma, Analysis and optimization of cross-flow

reactors with staged feed policies-isothermal operation with parallel-series, irreversible reaction systems, *Chem. Eng. Sci.* 52 (1997) 1349–1363.

- [59] Y. Lu, A.G. Dixon, W.R. Moser, Y.H. Ma, Analysis and optimization of cross-flow reactors with distributed reactant feed and product removal, *Catal. Today.* 35 (1997) 443–450.
- [60] H. Freund, K. Sundmacher, Towards a methodology for the systematic analysis and design of efficient chemical processes: Part 1. From unit operations to elementary process functions, *Chem. Eng. Process.* 47 (2008) 2051–2060.